Comparison of Solution Structures and Stabilities of Native, Partially Unfolded and Partially Refolded Pepsin†

Derek Dee,‡ Jeremy Pencer,§,|| Mu-Ping Nieh,§ Susan Krueger,⊥ John Katsaras,§,▽,# and Rickey Y. Yada*,‡,#

Department of Food Science, University of Guelph, Guelph, ON N1G 2W1, Canada, NRC-SIMS, Canadian Neutron Beam Centre, Chalk River Labs, Chalk River, ON K0J 1J0, Canada, Department of Physics, St. Francis Xavier University, P.O. Box 5000, Antigonish, NS B2G 2W5, Canada, NIST Center for Neutron Research, National Institute of Standards and Technology, 100 Bureau Drive, Bldg. 235/Room E151, Gaithersburg, Maryland 20899-8562, Department of Physics, University of Guelph, Guelph, ON N1G 2W1, Canada, and Biophysics Interdepartmental Group, University of Guelph, Guelph, ON N1G 2W1, Canada

Received June 25, 2006; Revised Manuscript Received September 15, 2006

ABSTRACT: A zymogen-derived protein, pepsin, appears to be incapable of folding to the native state without the presence of the prosegment. To better understand the nature of the irreversible denaturation of pepsin, the present study reports on the characterization of the stability and low-resolution tertiary and secondary structures of native, alkaline unfolded and acid refolded porcine pepsin. Through a combination of small-angle neutron scattering (SANS), CD, and DSC, acid refolded pepsin (Rp) was shown to have secondary and tertiary structures intermediate between the alkaline denatured and native forms but was found to be thermodynamically stable relative to the native state. It was also observed that the acid refolded state of pepsin was dependent on the protein concentration during refolding because CD and SANS data revealed that both the secondary and tertiary structures of concentrated-refolded pepsin (>10 mg/mL) (CRp) were native-like, in contrast to the intermediate nature of Rp, refolded under dilute concentration (<10 mg/mL). Despite a native-like conformation, CRp was more stable and had substantially reduced activity compared to that of the native state, suggesting that the protein was misfolded. It is proposed that the stable but misfolded, acid-refolded states are evidence that pepsin in its native conformation was metastable. Furthermore, the disruption of the active site cleft in the denatured states could be discerned by modeling of the SANS data.

Protein folding studies tend to focus on single domain proteins (*1*−*3*) that appear to conform to a two-state folding mechanism and are generally able to be reversibly unfolded. However, an interesting opportunity is presented by examining the unfolding and refolding of proteins that are inherently unable to refold to their native conformation, that is, they are unable to refold not because of extraneous circumstances (such as aggregation) but because of a lack of folding competence within the primary sequence. Proteins that do not appear to obey Anfinsen's rule (*4*) and are unable to refold to the native structure may be useful models for the study of folding intermediates. Many members of the peptidase family of enzymes fit this latter description (*5*−*8*).

Most peptidases known to date are produced as zymogens, containing a prosegment domain that is removed from the main enzyme body upon activation. Although the nature of the prosegment function is not entirely understood, it is evident that many peptidases require the presence of the prosegment in order to fold to the native structure (*9*).

Pepsin A belongs to the family of aspartic peptidases (*10*) and is synthesized at neutral pH as a zymogen containing a 44 residue prosegment. Through a variety of mechanisms (*11*), pepsin is capable of autoactivation at acidic pH to yield a mature enzyme of approximately 34.6 kDa (*12*). As a gastric enzyme, pepsin displays optimum activity in the pH range from 1−4 but has minimal activity above pH 5. Native pepsin contains a predominantly β-strand secondary structure and has a bilobal conformation with two catalytic Asp residues on either side of the active site cleft, formed between the *N*- and *C*-terminal domains (*13*) (Figure 1). Unlike pepsin, pepsinogen, the inactive, zymogen form of pepsin, can be reversibly unfolded by means of urea or alkaline pH (*14*, *15*). The irreversibility of pepsin unfolding has been the subject of a number of studies in the last few decades, but remains unsolved. Research by Amad and McPhie indicated that neutral pH denatured pepsin (in a covalently inhibited form) fully retained its disulfide linkages and,

† The financial support of the Natural Sciences and Engineering Research Council is gratefully acknowledged. This work utilized facilities supported in part by the National Science Foundation under Agreement No. DMR-0454672. We acknowledge the support of the National Institute of Standards and Technology, U.S. Department of Commerce, in providing the neutron research facilities used in this work. J.P., J.K., and M.-P.N. thank the Advanced Foods and Materials Network (Networks of Centres of Excellence, Canada) for financial assistance.

* Corresponding author. Phone: 1 (519) 824-4120 ext. 58915. Fax: 1 (519) 824-0847. E-mail: ryada@uoguelph.ca.

‡ Department of Food Science, University of Guelph.

§ Chalk River Labs.

|| St. Francis Xavier University.

⊥ National Institute of Standards and Technology.

▽ Department of Physics, University of Guelph.

Biophysics Interdepartmental Group, University of Guelph.

10.1021/bi061270i CCC: $33.50
Published on Web 11/01/2006

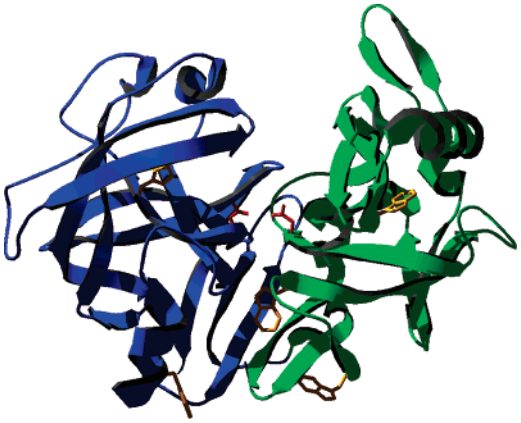

FIGURE 1: Crystal structure of pepsin (PDB code: 4PEP) as a ribbon representation, illustrating the bilobal structure of the *N*-(blue) and *C*-domains (green), which form the active site cleft. The catalytic residues Asp32 and Asp215 side chains are colored red, and the five Trp residue side chains are shown in orange.

furthermore, that a large amount of ordered structure persisted as further unfolding transitions could be brought about by the addition of Gdn-HCl (*16*) and also by urea (*17*). A calorimetric study by Privalov et al. suggested that the *N*- and *C*-terminal domains are independent folding units, with the *C*-terminal domain being much more stable and capable of reversible unfolding (*18*). It was later shown that only the *C*-terminal domain of alkaline pH denatured pepsin could form an active complex when combined with its recombinant partner domain (*19*). By introducing stabilizing mutations into the *N*-terminal domain, Tanaka and Yada (*20*) found that the rate of inactivation at pH 7.0 could be substantially reduced relative to wild-type inactivation; furthermore, by incorporating a disulphide bridge between the *N*-terminus and the bottom β-sheet plate (G2C/L167C), the complete alkaline denaturation of pepsin could be prevented even after many hours. Thus, prevention of the dissociation of the *N*-terminal lobe was related to the prevention of denaturation (*20*). More recent structural investigations, notably results from ^{1}H NMR, suggest that although the *N*-terminal domain contains relatively little organized structure, the *C*-terminal domain retains a compact and rigid, yet non-native, organization upon alkaline denaturation (*21*, *22*).

Through these previous studies, it has been established that neutral/alkaline pH denatured pepsin is partially unfolded (*16*, *17*, *21*, *22*), with the *N*-terminal domain undergoing more extensive loss of native structure compared to that of the *C*-terminal domain (*21*, *22*). The complete loss of activity and partial loss of secondary structure upon alkaline denaturation of pepsin has been fairly well documented (*16*, *17*, *21*−*24*), but there have been comparatively few studies of the tertiary structure of partially unfolded pepsin (*21*) as well as refolded conformations.

Despite a number of detailed crystallographic structural determinations of pepsin and related proteases, to the best of our knowledge, there has only been one small-angle scattering study characterizing the tertiary structure of pepsin in its native and alkaline denatured states (*21*). Previous small-angle X-ray scattering results (*21*) showed that the tertiary structure of pepsin changed on denaturation, but no definitive conclusions were made concerning the changes in tertiary structure during denaturation, nor were any measurements made to determine whether or not the tertiary structure of pepsin under renaturing conditions more closely resembles the denatured or native form. In the present study, small-angle neutron scattering (SANS[1]) and complementary techniques (CD, DSC, fluorescence, and densitometry) were used in order to resolve these issues.

Using different conditions of pH and protein concentration, the structure of pepsin under native (pH 5.3), denaturing (pH 8.0) and potentially renaturing (taken from pH 8 to pH 5) conditions was examined. Through ab initio modeling of the SANS data, the partially unfolded nature of the alkaline denatured state, the partially folded nature of the refolded state, and the native-like conformation of a concentrated-refolded pepsin sample were better defined. These states were further compared with secondary structure (CD), thermodynamic (DSC), and functional analysis.

MATERIALS AND METHODS

Materials. High purity porcine pepsin A (EC 3.4.23.1) was purchased from Sigma (St. Louis, MO) and used without further purification. The peptide substrate KPAEFF(NO_2)-AL was synthesized at the Core Facility for Protein/DNA Chemistry located at Queens University (Kingston, ON). Deuterium oxide (D_2O, 99.9%) was purchased from ACP Chemicals (Montreal, QC). Other chemicals were of reagent grade. (Reference to commercial sources and products used in this study does not constitute endorsement by the National Institute of Standards and Technology (NIST), nor should it be inferred that the products mentioned are necessarily the best available for the purpose used.)

Sample Preparation. Stock solutions of pepsin samples of known concentration (determined by mass and/or A_{280}, where E_{280} = 38,600 M^{-1} cm^{-1} (*21*)) were prepared and subsequently diluted in known volumes of the appropriate buffers. Pepsin was examined under three different conditions of pH using the following buffers: (a) 20 mM sodium acetate/acetic acid at pH 5.3 (native pepsin, Np), (b) 20 mM Tris/HCl at pH 8.0 (alkaline denatured pepsin, Ip), and (c) 1:1 mixture of 10 mM Tris/HCl at pH 8.0 and 40 mM sodium acetate/acetic acid at pH 4.7, with a final pH of 5.

Pepsin Refolding. In the preparation of pepsin in buffer c, a quantity of pepsin was first dissolved in one part 10 mM Tris/HCl at pH 8.0, incubated at 21 °C for at least 10 min, then further diluted with one part 40 mM sodium acetate/acetic acid at pH 4.7. Refolded samples for CD, DSC, and fluorescence experiments were prepared from alkaline unfolded (pH 8.0) pepsin samples ranging in concentration from 0.4−0.8 mg/mL (CD and fluorescence), from 0.8−1.6 mg/mL (DSC), and 5 mg/mL (SANS). These samples are referred to as refolded pepsin or Rp. For SANS, CD, and DSC experiments, refolded samples were also prepared from a 20 mg/mL alkaline unfolded pepsin solution. These samples are collectively referred to as concentrated refolded pepsin or CRp.

Kinetic Analysis. Kinetic measurements were taken using the octapeptide substrate KPAEFF(NO_2)AL (*25*) in which initial reaction rates ($-\Delta A$/min) were measured as the linear decrease in absorbance at 300 nm using a DU640 spectro-

[1] Abbreviations: SANS, small-angle neutron scattering; CD, circular dichroism; DSC, differential scanning calorimetry; Np, native pepsin; Ip, alkaline denatured pepsin; Rp, refolded pepsin; CRp, concentrated refolded pepsin.

photometer (Beckman Instruments, Fullerton, CA). At least 10 substrate concentrations were employed in the range of 0.002−0.16 mM octapeptide, with 10 nM pepsin. Initial reaction velocity data were plotted versus substrate concentration and fitted according to the Michaelis−Menton model using least-squares nonlinear regression analysis. Refolded samples were examined for activity using 10 nM protein and a single substrate concentration of 0.1 mM, at which 10 nM Np was found to approach V_{max}. Measurements were repeated at least in triplicate for each substrate concentration.

Small-Angle Neutron Scattering. SANS measurements were performed using the 30 m NG3 instrument located at the National Institute of Standards and Technology (NIST, Gaithersburg, MD). Three sample-to-detector distances, 13, 5, and 1.5 m were used with 5.5 Å ($\Delta\lambda/\lambda = 0.12$) neutrons to obtain a total range in scattering vector of $0.00637 < q < 0.4272$ Å^{-1}, where the scattering vector $q = 4\pi \sin(\theta/2)/\lambda$. Data were reduced and corrected for instrument response, empty cell scattering, and incoherent background and scaled to absolute intensity using the incident beam flux and the appropriate software provided by the NIST. The scattered intensity and its error correspond to the mean and standard deviation of the intensity averaged in rings of constant radial distance (corresponding to constant scattering vector, q) around the beam center on a 2D detector.

For SANS measurements, pepsin samples were prepared in both H_2O and D_2O buffers and diluted to a final concentration of 10 mg/mL (H_2O and D_2O) or 5 mg/mL (D_2O only). Protein solutions were then injected into cylindrical or banjo cells with 1 and 2 mm path lengths for H_2O and D_2O solutions, respectively. SANS measurements, typically lasting ~3 h per sample, were performed immediately after the dilution of the protein.

SANS data were analyzed using several routines belonging to a suite of analysis programs, ATSAS2.1, freely available from the Biological Small Angle Scattering Group (European Molecular Biology Hamburg Outstation, Hasylab). In particular, data were fitted and interpreted using the programs CRYSON (*26*), GASBOR (*27*), GNOM (*28*), and SASHA (*29*), which were used to compare SANS data to crystal structure predictions, produce low-resolution dummy residue models via fits by simulated annealing, calculate pair-distance distribution functions via the inversion of the SANS data, and produce model scattering envelopes by fits to data via spherical harmonic expansion of the protein scattering length density in real space, respectively. Data were also fit with the Guinier approximation to obtain radii of gyration, *R*g, using the Igor procedures provided by NIST.

*Densitometry***.** The densities of pepsin solutions and buffers were measured via the mechanical oscillator technique (*30*, *31*) with the use of two Anton Paar DMA 602 external cells using a DMA 60 measuring unit in the phase lock loop mode (Paar, A., and Graz, K. G., Austria). The temperature of the external cells was controlled by circulating thermostated fluid from a Neslab RTE-4 constant temperature bath. Instrument calibration and the determination of the densities of the various solutions were performed as described in refs 30 and 31 (*30*, *31*). The partial specific volume (υ) of pepsin at the various pH conditions was determined via the following equation:

$$\upsilon = [1 - (\rho_p - \rho_b)/c]/\rho_b \quad (1)$$

where υ is the specific volume of the protein, ρ_p is the density of the protein suspension, ρ_b is the density of the buffer, and c is the mass concentration of protein in solution. Measurements on each solution were performed at least in triplicate, and the results presented correspond to the mean and standard deviations of each condition.

Circular Dichroism Spectroscopy. Circular dichroism (CD) spectra were recorded using a Jasco J-600 spectropolarimeter (Japan Spectroscopic, Tokyo, Japan). Data were recorded in the far-UV range from 250−190 nm with a 1 nm bandwidth, 100 nm/min scan rate, 0.25 s response time, and 4× accumulation. In each case, 0.2 mg/mL of pepsin solution was analyzed in a cuvette with a 0.1 cm path length, and a minimum of three measurements were made per sample. Prior to each pepsin sample run, the corresponding buffer alone was run and was subtracted from the subsequent pepsin spectra before further analysis. All solutions were filtered and degassed before measurement. Ellipticity values recorded as a function of wavelength (λ) were converted into mean residue ellipticity $[\theta]_{mrw,\lambda}$ using the following equation:

$$[\theta]_{mrw,\lambda} = MRW \times \theta_\lambda/10 \times d \times c \quad (2)$$

where *MRW* is the mean residue weight (107 g/mol for pepsin (*23*)), θ_λ is the measured ellipticity at a particular wavelength (degrees), d is the path length (0.1 cm), and c is the protein concentration (g/cm^3).

Differential Scanning Calorimetry. Calorimetry experiments were carried out with a MicroCal VP-DSC (MicroCal, Northampton, MA) using a scan rate of 1.5 °C/min over a temperature range from 10−110 °C, 16 s filtering period (time delay), and passive feed-back response. The final concentration of pepsin samples used was ~0.4 mg/mL, with the corresponding buffer used as the reference. Data reduction and analysis were performed using MicroCal Origin v7.0 (OriginLab, Northampton, MA).

Intrinsic Fluorescence. Fluorescence spectra were recorded using a Shimadzu RF-540 spectrofluorophotometer (Shimadzu Corporation, Kyoto, Japan) with a 1-cm quartz cell at room temperature and the following settings: excitation at 295 nm (the optimal excitation wavelength for measurements of Trp fluorescence), emission scan from 305−450 nm, and excitation and emission slit widths of 5 nm. All samples consisted of 0.20 mg/mL pepsin (5.8 μM) and were measured at least in triplicate.

RESULTS

Pepsin Behavior in H_2O and D_2O. Critical to the investigation of pepsin conformation by SANS, was the comparison of the behavior of pepsin in D_2O and H_2O. Typically, neutron scattering measurements of proteins are performed with buffers composed of 100% D_2O because of both improved signal-to-noise and increased contrast compared to measurements in H_2O. However, some proteins are observed to display anomalous behavior in pure D_2O (*32*−*34*). Thus, prior to SANS studies, it was necessary to verify that pepsin retained native activity, that is, native conformation, in a deuterated solution.

The behavior of pepsin in D_2O versus H_2O was monitored through kinetic studies, which yielded similar ($p > 0.05$) results for both solvents, with k_{cat}/K_m values of 1.6 ± 0.6 and 2.3 ± 0.7 s^{-1} μM^{-1} for pepsin in H_2O and D_2O,

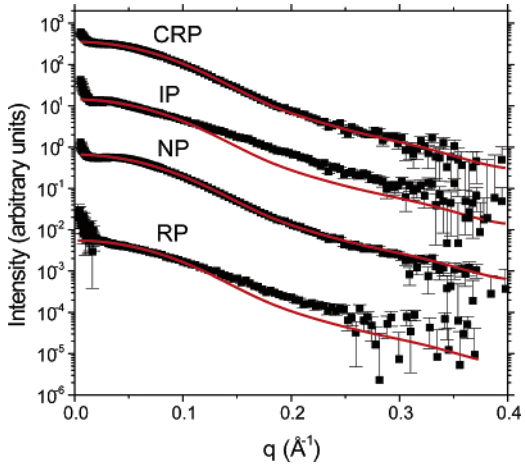

FIGURE 2: SANS curves for Np (pH 5.3), Ip (pH 8.0), Rp (pH 8 → 5, low protein *c*), and CRp (pH 8 → 5, high protein *c*) in D_2O buffer. Both the experimental (■) and theoretical (calculated from the crystal structure, 5PEP) (solid red curve) data are shown. Curves are offset along the *y*-axis for clarity.

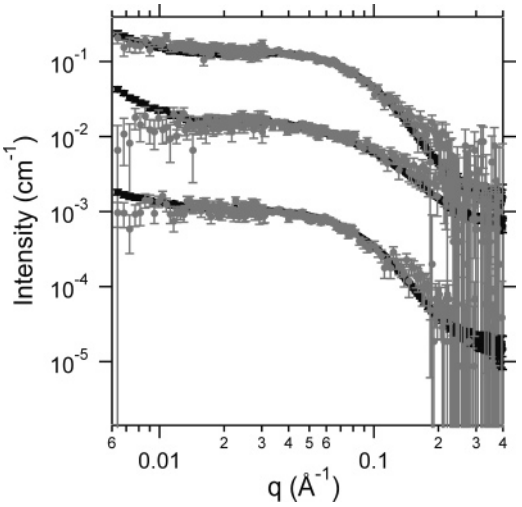

FIGURE 3: SANS curves for pepsin in D_2O (black symbols) overlaid with those in H_2O (gray symbols): Np, top; Ip, middle; and CRp, bottom.

respectively. Calorimetric measurements of pepsin showed similar heat capacity profiles of the native protein in the two solvents, although the melting transition in D_2O (67.61 ± 0.19 °C) was significantly ($p \leq 0.05$) greater than that in H_2O (62.16 ± 0.29 °C), implying that D_2O had a slight stabilizing effect (*35*, *36*). For pepsin under unfolded, dilute, and concentrated refolded conditions, the heat capacity profiles did not appear to change substantially with isotopic conditions. Although the absolute intrinsic fluorescence of the Trp residues of pepsin appeared to be higher in D_2O compared to that in H_2O, the spectral changes that accompanied the structural changes of pepsin were similar in the two solvents. The secondary structure and changes in structure revealed by CD appeared to be independent of the isotopic composition of the medium. Finally, the SANS results, discussed below, indicated little difference between pepsin in H_2O and D_2O, with the exception of the improved signal-to-noise and increased contrast in D_2O.

Small-Angle Neutron Scattering

Comparison of SANS Results to the Crystal Structure. As described in Svergun et al. (*26*) (and references therein), the program CRYSON calculates a SANS profile from the crystal structure of a protein. The program can also be used to fit small-angle scattering data by combining the calculated SANS profile with varying thicknesses or densities of a bound water layer and levels of incoherent background. CRYSON was used to determine the SANS profile from the crystal structure of pepsin (5PEP). In comparing the predicted SANS profile to those obtained experimentally, the incoherent background and thickness of the bound water layer in CRYSON were fixed to be zero.

In Figure 2, the predicted scattering curve is shown plotted against the experimental results for Np, Ip, Rp, and CRp. The SANS curves obtained from pepsin in D_2O showed enhanced forward scattering or an upswing in the intensity at low *q*, indicative of either protein aggregates or protein−protein interactions (*37*, *38*). Figure 3 shows plots, at each pH condition, of the scattering curves obtained in H_2O superimposed over those taken in D_2O. A comparison of the scattering curves for each pH condition showed that for $q \geq 0.03$ Å^{-1}, the scattering curves from pepsin in D_2O matched those in H_2O, demonstrating that neither the protein aggregate of the interparticle structure factor influenced the scattering curves in this range. Rp was also examined in pure H_2O; however, these data are not shown because the coherent signal was too low with respect to the incoherent background to resolve.

In contrast to pepsin in D_2O, the low *q* data of pepsin in H_2O exhibited poor signal-to-noise ratios at the long sample-to-detector distance (13 m), the result of increased incoherent scattering and a reduced incident neutron flux. Noise at high *q* for data taken both from pepsin in H_2O and D_2O reflected the small contribution to the scattering from pepsin relative to the incoherent background. For the analysis and discussion presented below, only the data in the range $0.034 < q < 0.26$ Å^{-1} for samples in D_2O and $0.034 < q < 0.2$ Å^{-1} for samples in H_2O were considered. The limits on *q* were intended to eliminate potential artefacts that could be introduced at low *q*, either by aggregates or by interparticle interactions (*39*), whereas at high *q*, they were introduced by poor counting statistics due to the small contribution to scattering from pepsin relative to the incoherent background.

For samples in pH 5.3 solution, the experimentally measured SANS curves for pepsin clearly matched that predicted from the crystal structure. When pepsin was in its denatured form at pH 8, the measured SANS curves followed the predicted SANS profile at low *q* but diverged above $q = 0.1$ Å^{-1}, demonstrating that the denaturation of pepsin led to a substantial change in the tertiary structure, as was observed previously by Konno et al. (*21*). When the denatured protein was titrated from pH 8 back to pH 5 under dilute protein concentration ($c < 10$ mg/mL), comparison between the experimental and predicted scattering curves showed that pepsin did not recover its native tertiary structure. In comparison, pepsin refolded at higher concentration ($c > 10$ mg/mL) was characterized by a native-like tertiary structure.

Pepsin Radii of Gyration via Guinier Plots

Guinier plots and the corresponding fits to the scattering data from Np, Ip, Rp, and CRp in D_2O are shown in Figure

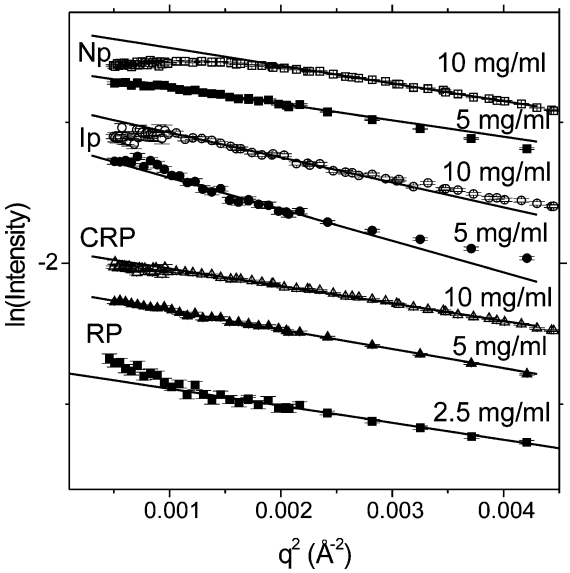

FIGURE 4: Guinier fits to the SANS data for Np, Ip, Rp, and CRp states in D_2O.

Table 1: Radii of Gyration (*R*g) Obtained[a] from the Guinier Approximation of the Scattering Data

	c (mg/mL)	*R*g (Å)	fitting range	norm. χ^2
Np (pH 5.3)	10	19.5 ± 0.2	0.99 < *q*Rg < 1.3	1.2
	5	19.8 ± 0.2	0.67 < *q*Rg < 1.1	2.0
Ip (pH 8.0)	10	22.6 ± 0.3	0.68 < *q*Rg < 1.1	1.3
	5	29.3 ± 0.7	0.81 < *q*Rg < 1.3	1.2
Rp (pH 8 → 5)	2.5	19.9 ± 0.3	0.55 < *q*Rg < 1.3	1.3
CRp (pH 8 → 5)	10	19.4 ± 0.1	0.70 < *q*Rg < 1.3	0.93
	5	20.3 ± 0.2	0.37 < *q*Rg < 1.0	0.62

[a] Values ± SD determined from single linear regression fits of SANS data.

4. The *R*g values obtained from the fits are given in Table 1. The denaturation of pepsin at pH 8 led to an increase in *R*g, whereas the titration of alkaline denatured pepsin back to pH 5 returned *R*g to its original value. Noteably, *R*g for Ip was found to be greater at 5 mg/mL protein concentration than at 10 mg/mL. It is likely that *R*g determined at 10 mg/mL was underestimated because of the influence of the protein structure factor. Because of the protein charge being higher at pH 8 than at pH 5 (∼ −38 and −17, respectively (*40*)), it was speculated that the protein structure factor for Ip would be more pronounced and, thus, more sensitive to protein concentration than that for Np, Rp, or CRp. The above may explain why a concentration effect on *R*g was observed for Ip but not for the Np and refolded states.

Kratky Plots

A qualitative method for assessing protein structure, utilizing the asymptotic behavior of the scattering function at high *q*, is possible by replotting the data as q^2I versus *q*, commonly known as a Kratky plot (*41*). For globular proteins, the scattering decays as q^{-4}, whereas for proteins that are completely unfolded, that is, are random coil structures, the scattering decays as q^{-2}. Kratky plots will show a plateau region at high *q* in the case of random coil structure or a peak at finite *q* followed by a monotonic decrease in the case of globular structure (*41*). An examination of Kratky plots (Figure 5) of the SANS data for pepsin

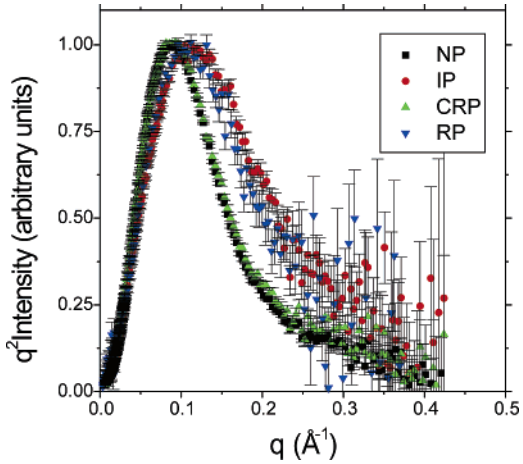

FIGURE 5: Kratky plots, showing q^2I vs *q* for Np, Ip, Rp, and CRp in D_2O. The curves are normalized with respect to their maximum values.

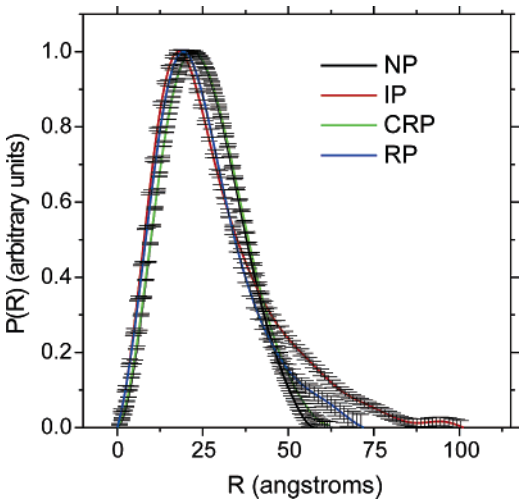

FIGURE 6: Pair distance distribution functions, *P*(*R*), for pepsin in D_2O (Np and CRp curves overlap).

in its native, partially unfolded and dilute, and concentrated refolded states indicated that the protein was globular in all four states.

Pair Distance Distribution Function, P(R)

The pair-distance-distribution function, or *P*(*R*), is obtained from a model independent transformation (*42*) of small-angle scattering data and essentially describes the scattering length density weighted correlation between mass elements within a protein (*39*). The *P*(*R*) curves evaluated from the SANS data are shown in Figure 6. Again, the data in D_2O and H_2O (data not shown) were not substantially different; however, an analysis of *P*(*R*) curves obtained for pepsin in H_2O was not useful because of the poor resolution and additional noise in the case of H_2O. The *P*(*R*) for Ip and Rp were found to differ from that for Np and extended to a D_{max} of ∼100 and ∼72 Å, respectively, whereas that for CRp was essentially the same as that of the native form (D_{max} ∼60 Å), consistent with the observations above.

Low-Resolution Structure via Dummy Residue Models: GASBOR

Using the *P*(*R*) profiles obtained by GNOM, it was possible, via simulated annealing fits, to obtain a low-

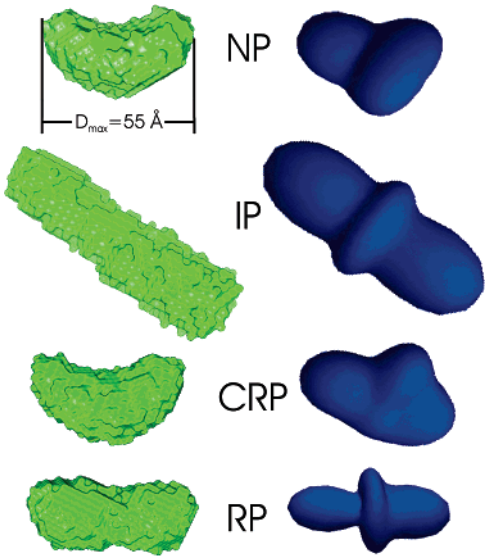

FIGURE 7: Low resolution (i.e., $r > 10$ Å) models of four states of pepsin, based on scattering data, calculated using (left side) a dummy residue model based on simulated annealing and fits of the $P(R)$ curve, GASBOR, and (right side) a model using spherical harmonics approximation of the protein scattering density, SASHA.

resolution dummy residue model representation of pepsin. Because a single structural solution to the SANS data obtained by this method need not be unique, the most generally accepted approach is to obtain a set of solutions from which an average is obtained (*27*). Because the SANS data obtained for pepsin in H_2O had a narrower range of usable q data but showed no considerable difference from that obtained in D_2O, only the D_2O data were fit. On the left side of Figure 7, dummy residue representations of structures for Np, Ip, Rp, and CRp are shown.

The overall shape of Np determined by GASBOR was found to be qualitatively similar to that of the crystal structure, with the bilobal and active-site cleft features partially resolved. However, the structure of Ip was found to be quite different, that is, elongated and nearly cylindrical. Again, consistent with the results presented above, it was shown that CRp had a tertiary structure that closely matched that of native pepsin, whereas that for Rp was intermediate between the Ip and Np forms.

Low-Resolution Structure via Scattering Envelopes: SASHA

As an alternative to the simulated annealing procedure, a low-resolution protein structure can be determined using a method in which the real space representation of the protein scattering length density is approximated by a sum of spherical harmonics, which are used to calculate Fourier coefficients used to fit the scattering data (*29*). Although GASBOR utilizes the $P(R)$ function determined by GNOM, SASHA fits the experimentally determined SANS profiles directly. Thus, SASHA represents a complementary analysis method. On the right side of Figure 7, visual representations of the scattering envelopes determined by SASHA fits are shown alongside the results obtained using GASBOR, with the structures produced from both methods found to be in close agreement. Again, Np showed a compact, bilobal shape, Ip showed an extended, rod-like conformation, and Rp appeared to recover some tertiary structure, whereas CRp had a native-like conformation.

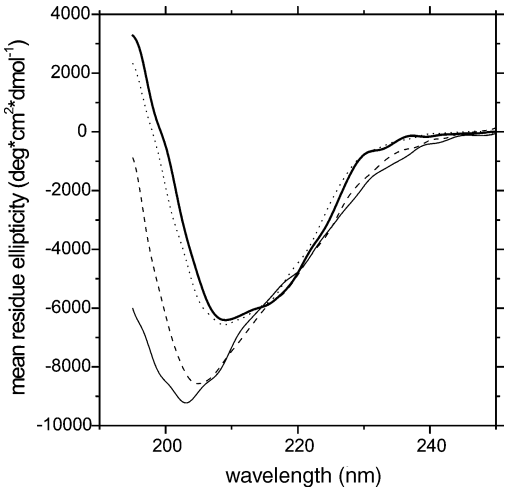

FIGURE 8: Comparison of circular dichroism spectra from pepsin (0.2 mg/mL; H_2O buffer) in four conformational states: (1) Np at pH 5.3 (bold, solid line); (2) Ip at pH 8.0 (thin, lowest solid line); (3) Rp at pH 5 (dashed line); and (4) CRp at pH 5 (dotted line).

Partial Specific Volume. Under certain conditions, the conformational change of a protein can be accompanied by substantial changes to its apparent partial specific volume. β-Lactoglobulin, for example, showed close to a 10% increase in v upon denaturation in 10% hexafluoroisopropanol solution (*43*). Our densitometry measurements of pepsin, however, showed no significant difference ($p > 0.05$) among three states of the protein. The Np, Ip, and CRp states had specific volumes of 0.784 ± 0.040, 0.782 ± 0.004, and 0.784 ± 0.010 cm^3/g, respectively.

Circular Dichroism Analysis. In order to determine possible conformational changes on smaller length scales (i.e., changes to secondary structure), circular dichroism spectra were collected from pepsin under native, unfolded, and two refolded conditions (Figure 8).

Examination of the CD spectra (Figure 8) clearly showed a shift in the minimum of the mean residue ellipticity (MRE) from ~210 nm to ~204 nm when going from pH 5.3 (native) to pH 8 (unfolded). The shift in MRE was qualitatively consistent with a loss of β-sheet structure in favor of random coil structure (*23*). The spectrum for Rp differed slightly from that of the Ip state, suggesting that a small portion of organized structure was reformed, whereas that for CRp matched closely with the native spectra, suggesting a greater recovery of secondary structure. Secondary structure proportions were estimated using three different algorithms (SELCON3 (*44*), CONTINLL (*45*), and CDSSTR (*46*)), each with two different protein reference sets (set 4 and 7, where set 7 contains data from four denatured proteins) via the DICROWEB server (*47*, *48*). Results from estimates that gave a normalized root-mean-square deviation from the experimental data of less than 0.25 were accepted (*49*) and averaged to give the final estimate of secondary structure (Table 2). The α-helical and β-turn content remained more or less unchanged upon unfolding and refolding; however, there was a significant ($p \leq 0.05$) loss of strand and concurrent increase in unordered structure upon alkaline denaturation. Interestingly, either a partial or nearly complete reversal of this process was observed upon dilute or concentrated refolding, respectively.

Intrinsic Tryptophan Fluorescence. Trp-fluorescence was used to monitor the conformational changes of pepsin upon

Table 2: Secondary Structure Estimated from the CD Spectra for Np (pH 5.3), Ip (pH 8.0), Rp (pH 5), and CRp (pH 5) in H_2O and D_2O[a]

	helix (%)	strand (%)	turn (%)	random (%)
Np, $_{H2O}$	$8.2 \pm 2.9_{A}$	$38.6 \pm 4.9_{A}$	$22.4 \pm 1.4_{A}$	$28.3 \pm 3.6_{A}$
Ip, $_{H2O}$[b]	$9.7 \pm 2.3_{A}$	$23.8 \pm 3.8_{B}$	$21.0 \pm 4.5_{A}$	$46.1 \pm 10.4_{B}$
Rp, $_{H2O}$	$9.9 \pm 2.5_{A}$	$30.8 \pm 2.8_{C}$	$21.4 \pm 1.3_{A}$	$37.4 \pm 5.2_{B}$
CRp, $_{H2O}$	$12.4 \pm 7.1_{A}$	$38.1 \pm 0.6_{A}$	$20.7 \pm 3.9_{A}$	$28.2 \pm 3.6_{A}$
Np, $_{D2O}$	$12.2 \pm 6.3_{A}$	$38.5 \pm 0.4_{A}$	$20.8 \pm 3.6_{A}$	$28.2 \pm 3.3_{A}$
Ip, $_{D2O}$	$6.6 \pm 2.3_{A}$	$28.6 \pm 4.4_{B,C,E}$	$21.1 \pm 3.7_{A}$	$43.2 \pm 9.1_{B}$
Rp, $_{D2O}$[c]	$9.2 \pm 2.7_{A}$	$32.5 \pm 2.2_{C,D,E}$	$21.9 \pm 0.6_{A}$	$35.5 \pm 5.3_{B,C}$
CRp, $_{D2O}$[c]	$8.9 \pm 2.0_{A}$	$33.8 \pm 1.8_{D}$	$22.3 \pm 0.7_{A}$	$35.0 \pm 2.5_{C}$

[a] Values are given as the mean ± SD of six (or five where noted) separate estimates. Means in each column sharing the same letter are not significantly different, $p > 0.05$. [b] Five estimates: SELCON3, reference set 4 results omitted. [c] Five estimates: SELCON3, reference set 7 results omitted.

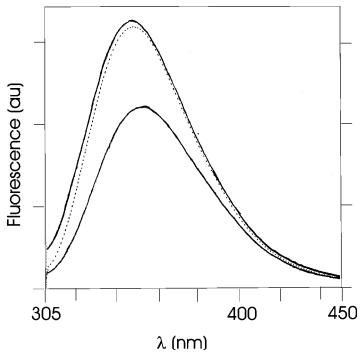

FIGURE 9: Fluorescence spectra for pepsin (5.8 μM) in three different states: (1) Np at pH 5.3 (solid, uppermost curve); (2) Ip at pH 8.0 (solid, lowest curve); and (3) Rp at pH 5 (dotted curve).

Table 3: Fluorescence Spectral Parameters[a] for Pepsin in H_2O and D_2O Buffer

condition (pH)	λ_F (nm)	F	$F_{relative}$ (%)
Np, $_{H2O}$	$348.0 \pm 0.8_{A,D}$	$67.8 \pm 2.6_{A,E}$	100
Ip, $_{H2O}$	$352.3 \pm 0.2_{B}$	$49.1 \pm 3.2_{B}$	72
Rp, $_{H2O}$	$349.0 \pm 0.7_{A}$	$65.1 \pm 1.3_{A}$	96
Np, $_{D2O}$	$348.0 \pm 0.3_{A}$	$76.9 \pm 5.5_{C}$	100
Ip, $_{D2O}$	$351.2 \pm 0.5_{C}$	$57.4 \pm 8.1_{D}$	75
Rp, $_{D2O}$	$346.6 \pm 0.4_{D}$	$68.3 \pm 0.5_{C,E}$	89

[a] Means in each column sharing the same letter are not significantly different, $p > 0.05$.

unfolding and refolding. The transfer of Trp from a polar to nonpolar environment results in a blue shift of the fluorescence emission. Conversely, exposure to aqueous solution of previously buried Trp residues will be reflected by a red shift in the emission spectrum (for further reading, refer to ref 50 (*50*)). The fluorescence spectra for pepsin in three states (Np, Ip, and Rp) are given in Figure 9. A comparison of the maximum fluorescent intensities (F) and their corresponding wavelengths (λ_F) (Table 3) showed that for Ip, F decreased to ~72% of the value for Np and was red-shifted by ~3 nm. Refolding of the denatured pepsin gave a spectrum characteristically very similar to that of the native pepsin in that F was increased and λ_F was blue-shifted relative to the Ip state. Furthermore, the λ_F values suggested (*51*) that those Trp residues that contributed substantially to the spectra for Np and Rp were partially exposed, whereas those for Ip were completely exposed to the solvent.

Differential Scanning Calorimetry. As shown below (Table 4), DSC measurements were used to assess the conformational stability of the various states of pepsin. For all but the Ip samples, the excess heat capacity scans gave rise to two apparent melting events (termed here peak one, P1 and peak two, P2). P2 was assumed to correspond to the main melting or unfolding transition of both pepsin domains, whereas the origin of P1 remains unclear. Although two separate melting transitions of pepsin have previously been observed and associated with the independent unfolding of the *N*- and *C*-terminal domains (*18*), that possibility was ruled out for these measurements. In contrast to results reported by Privalov et al. (*18*), where the *N*- and *C*-domain melting transitions were of comparable enthalpy and the two transitions converged to a single transition for pepsin samples below pH 6, the calorimetric enthalpy (ΔH^{cal}) of P1 was nearly 1/10th the magnitude of that for P2 (Table 4). Furthermore, in some heat capacity profiles, P1 appeared to more closely resemble a step in the heat capacity profile than an actual peak, and therefore, it was unclear whether P1 corresponded to an unfolding transition.

Figure 10 shows the heat capacity profiles measured from heating scans of pepsin under the various conditions (in H_2O). It was found that Np gave a fairly sharp, high enthalpy transition relative to Ip, which showed a much broader transition with lower enthalpy and a concomitantly lower transition temperature (T_m). Measurements by DSC revealed further differences between Rp and CRp. In the case of the concentrated-refolded protein, the transition was narrow, with a width and enthalpy comparable to those of the native state. The T_m of CRp was found to be significantly ($p \leq 0.05$) higher than that of the native state, indicating a conformational difference between the native and concentrated refolded states of pepsin. In the dilute-refolded case, the heat capacity profile was quite low and broad, although there was also a significant ($p \leq 0.05$) shift of T_m to a higher value than that observed for Np.

Figure 11 shows the first scan of Np along with the second, third, and fourth re-scans of the same sample. Although the Np transition was found to be irreversible, with a second scan showing a transition with only ~20% ΔH^{cal} of the original transition, the second scan gave an excess heat capacity profile similar to that for Rp. Successive heating scans of the melted Np sample revealed that this transition was highly reversible, giving 95% and 85% of the initial ΔH^{cal} on the second and third scans, respectively. In addition, Np samples taken from the DSC after the first heating/cooling cycle were analyzed by CD and yielded spectra (not shown) similar to those of Rp.

The ratio of the calorimetric enthalpy (ΔH^{cal}) to the van't Hoff enthalpy (ΔH^{vh}) can be taken as a measure of the cooperativity of protein unfolding (*52*). A $\Delta H^{cal}/\Delta H^{vh}$ ratio of one indicates a completely cooperative and two-state unfolding process, whereas any deviation from unity indicates either a reduction in cooperatively (i.e., cooperative units smaller than the whole protein) or a non-two-state behavior of the protein (*52*). $\Delta H^{cal}/\Delta H^{vh}$ ratios were estimated by fitting the Np, CRp, and Rp endotherms (in H_2O) with a single non-two-state transition, yielding values of 1.36 ± 0.08, 1.17 ± 0.04, and 1.02 ± 0.07, respectively. The larger $\Delta H^{cal}/\Delta H^{vh}$ for Np compared to that for CRp suggested that unfolding of CRp was slightly more cooperative, whereas

Table 4: Parameters[a] Derived from the DSC Scans of the Various States of Pepsin (Np, Ip, Rp, and CRp) in Both H_2O and D_2O Buffers, for Either One or Two Transitions Where Observed

sample	T_{m1} (°C)	ΔH_1^{cal} (kcal/mol)	T_{m2} (°C)	ΔH_2^{cal} (kcal/mol)
Np, $_{H2O}$	33.63 ± 1.53 $_{A}$	10.55 ± 2.25 $_{A}$	62.16 ± 0.29 $_{A}$	176.72 ± 2.32 $_{A}$
Ip, $_{H2O}$			56.47 ± 0.48 $_{B}$	42.83 ± 1.33 $_{B}$
Rp, $_{H2O}$	35.04 ± 1.83 $_{A,B}$	6.70 ± 2.14 $_{B}$	67.00 ± 2.05 $_{C, D}$	44.67 ± 4.27$_{B}$
CRp,$_{H2O}$	35.82 ± 1.51 $_{A,B}$	26.66 ± 6.41 $_{C}$	65.11 ± 0.13 $_{C}$	152.83 ± 3.05 $_{C}$
Np, $_{D2O}$	35.17 ± 0.54 $_{A,B}$	11.98 ± 2.20 $_{A}$	67.61 ± 0.19 $_{D}$	157.83 ± 15.96 $_{A,C}$
Ip, $_{D2O}$			61.95 ± 0.34 $_{A}$	42.05 ± 1.98 $_{B}$
Rp, $_{D2O}$	37.21 ± 1.98 $_{B}$	9.99 ± 6.01 $_{A, B}$	63.68 ± 3.09 $_{A, C}$	20.94 ± 4.19 $_{H}$
CRp,$_{D2O}$	35.97 ± 0.42 $_{A,B}$	12.14 ± 1.97 $_{A}$	71.03 ± 0.22 $_{E}$	161.39± 11.39 $_{C}$

[a] These parameters were obtained by integrating the area between the baseline (created as a cubic curve) and the experimental curve. Obtaining data in this way assumes $\Delta C_p = 0$ for the transitions. The values were determined as the mean ± SD from at least three separate DSC scans. The means in each column sharing the same letter are not significantly different, $p > 0.05$.

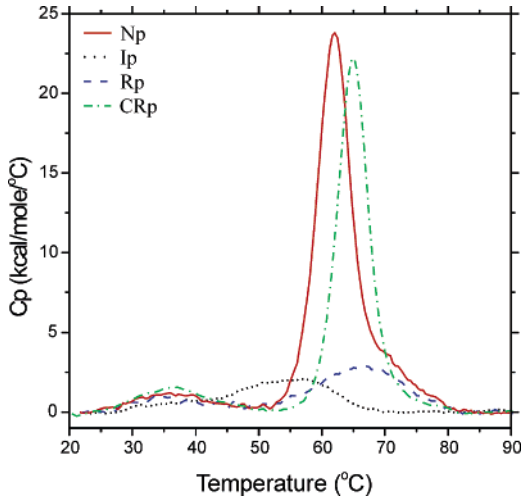

FIGURE 10: Four conformations of pepsin as observed by DSC. Endotherms shown are for Np, Ip, Rp, and CRp, after the subtraction of a reference scan and a baseline.

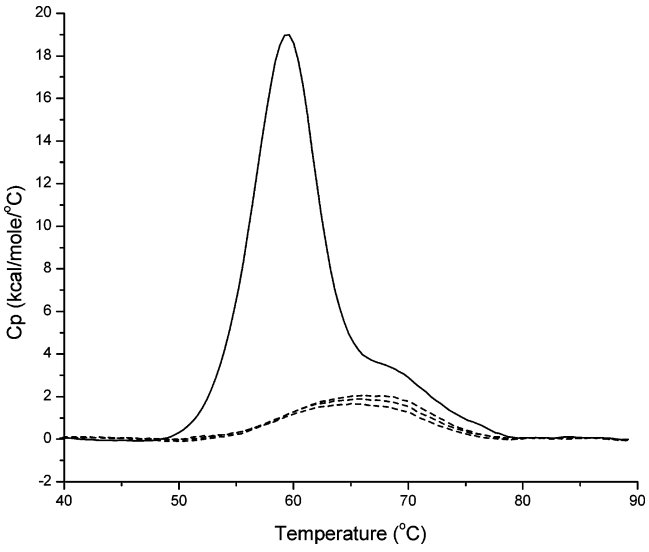

FIGURE 11: Irreversibility of Np unfolding by DSC. Upon cooling after the first scan of Np (solid curve), the second, third and fourth scans (broken curves) were highly reversible.

Rp unfolding was substantially more cooperative than that of Np. Overall, the data suggested that unlike Rp, the unfolding of both CRp and Np proceeded through a non-two-state mechanism.

Although the transitions did not ideally follow two-state behavior, their approximation as a two-state transition (*5*) allowed for the comparison of the relative thermodynamic stability of Np and CRp with that of Rp. Fitting the endotherms from Np, CRp, and Rp (in H_2O) with a single two-state transition, the resulting values of T_m, $\Delta H(T_m)$, and heat capacity change at the transition midpoint, $\Delta C_p(T_m)$, were used to calculate apparent Gibbs free energy values, ΔG_{app}. Previous studies of Gdm-HCl denaturation of pepsin monitored by activity and absorbance (300 nm) yielded an apparent free energy value of $\Delta G_{app} = 5.42 \pm 0.36$ kcal/mol (25 °C) (*53*), which is in close agreement with the value for Np (4.85 ± 0.58 kcal/mol) determined in the present study. ΔG_{app} (25 °C) for CRp (11.19 ± 0.95 kcal/mol) was roughly twice that of Np, whereas that for Rp (5.75 ± 0.41 kcal/mol) was slightly higher, demonstrating that both CRp and Rp were significantly ($p \leq 0.05$) more stable than Np.

Refolded Pepsin Activity. Activity measurements were made on refolded pepsin samples as described above. Although Rp displayed no activity, CRp gave an initial rate of $-\Delta A/\text{min} = 0.012 \pm 0.003\ \text{min}^{-1}$. For comparison, Np had a significantly greater ($p \leq 0.05$) initial rate of $-\Delta A/\text{min} = 0.031 \pm 0.005\ \text{min}^{-1}$ under the same conditions. Thus, the activity of CRp was found to be about 39% of that of the native form.

DISCUSSION

Unfolding. The present study confirmed and supports previous (*21*) research regarding the Ip state of pepsin. Similar to results reported by Konno et al. (*21*), an increase in *R*g was found upon alkaline unfolding (from ~20 Å to ~30 Å). Although enzymatically inactive at pH 8, pepsin still retained a high degree of secondary structure, exhibited a globular rather than random coil conformation, and underwent a heat induced enthalpic unfolding transition. In particular, ab initio modeling of the SANS data illustrated the nature of the Ip conformation as being relatively compact yet distinctly elongated relative to that of Np, Rp, and CRp.

The Ip state was partially unfolded because CD measurements indicated a loss of β-strand and an increase in random structure, in agreement with previous studies (*17*, *21*, *23*). Also, DSC measurements showed that the melting transition of Ip was much broader, decreased in T_m, and had a reduced enthalpy compared to that of Np. However, the heat capacity profile demonstrated that Ip still retained residual structure, which was denatured on heating.

SANS measurements showed a retention of tertiary structure via Guinier plots (Figure 4) and low-resolution

structural reconstruction (Figure 7), which showed that the Ip state was still comparatively compact, and by Kratky plots (Figure 5), which indicated that although Ip differed from Np, it still retained globular features. Densitometric measurements also showed that there was no difference in the apparent partial specific volume of Ip and Np, though it is not clear a priori whether a protein should always show a volume expansion upon denaturation (*30*, *43*).

In an earlier functional study (*19*), in which pepsin activity was recovered by the addition of recombinant *N*-terminal domain of pepsinogen to denatured pepsin (Ip), it was postulated that the *C*-terminal domain retained its native structure in the Ip state. From recent structural investigations (*21*, *22*), it was shown that the *C*-terminal lobe of Ip had non-native secondary structure and, furthermore, that the *N*-terminal lobe did retain some degree of nonrandom structure. From the SANS data in the present study, it appeared that the *N*-terminal lobe of pepsin was not fully unfolded because Kratky plots indicated a relatively compact form for the Ip state with no apparent contribution to the scattering profile from a random coil conformation. Furthermore, from the models produced by SASHA, and in particular GASBOR (Figure 7), it appeared that both *N*- and *C*-domains may have undergone unfolding as the two domains separated. The results of Lin et al. (*19*) and Privalov et al. (*18*), rather than suggesting a native *C*-domain in the Ip state, may support the notion that the *C*-domain retains the ability to refold and form a functional domain, whereas the *N*-domain is incapable.

Refolding. Relative to that of the Ip state, information available in the literature on the structure of refolded pepsin is limited and somewhat conflicting. Some studies (*16*, *24*) have reported that alkaline denatured and subsequently acid refolded pepsin generated a CD spectrum very similar to the native spectrum, while it has recently been reported that refolded pepsin did not give a native-like CD spectrum (*21*). Measurements by CD (Figure 8) and DSC (Figure 10) showed that the refolding of pepsin was concentration dependent. Two regimes of pepsin refolding were carried out, one with dilute Ip (<10 mg/mL) and the other with concentrated Ip (>10 mg/mL), yielding two distinct refolded states of pepsin, that is, Rp and CRp. Both the secondary and tertiary structures of Rp were intermediate between the Np and Ip forms and, using DSC showed a reversible, low enthalpy transition that was approximately two-state. In contrast, CRp exhibited secondary and tertiary structures similar to those of Np but with a greater conformational stability. Although the concentrated refolding of pepsin from the Ip state led to nearly complete recovery of both its secondary and tertiary structures, it was found that CRp had considerably lower activity for the synthetic substrate than Np, suggesting that CRp was misfolded with respect to the native state.

To our knowledge, this is the first article on the tertiary structure of pepsin under potentially renaturing conditions. The partially unfolded conformation of the Ip state has been characterized as remaining globular yet extended. Combined with the findings that both domains contain non-native structure (*21*, *22*), it is hypothesized that the two domains unfold while separating, as supported by the models in Figure 7. Re-acidifying the alkaline denatured state was shown (Figure 7) to result in a partial reversal of this process. In the Rp state, it appeared that both domains became more compact. Furthermore, the fluorescence spectrum of Rp was similar to that of Np (Table 3), which also indicated that Rp was more compact than Ip.

Comparison of the DSC heat capacity profiles of Rp, CRp, and Np (Figure 10; Table 4) revealed that both Rp and CRp had higher T_m values, suggesting (*54*) that the refolded states had a greater conformational stability than that of Np. Calculation of an apparent Gibbs free energy change of unfolding (ΔG_{app}) further supported that Rp and CRp were thermodynamically more stable than Np. However, the transitions for Np and CRp were both completely irreversible in that after the first melting and cooling cycle of Np or CRp samples, successive heating scans produced excess heat capacity profiles similar to those of Rp. Furthermore, Np samples that were heated and cooled by DSC gave CD spectra identical to that of Rp. Thus, it was observed that upon melting Np and cooling the sample, Rp was formed, indicating that the Rp state could be formed both by thermal and pH induced unfolding/refolding of pepsin. Thus, it is hypothesized that Np at pH 5.3 represents a metastable state, whereas Rp represents a truly thermodynamically stable state.

The findings reported in the present study and elsewhere (*16*, *21*, *24*) have shown that for equivalent final conditions, different refolded states of pepsin could be observed depending on the initial conditions (e.g., buffer, pH, protein concentration, etc.) before/during refolding. From a thermodynamic perspective, the starting conditions should not determine the final folded state, only the final conditions (*55*); thus, the present results are suggestive of a strong kinetic influence on the folding mechanism of pepsin.

A comparison of the initial calorimetry data for Np with that of Rp and CRp suggests that non-native conformations of pepsin exist, which are thermodynamically more stable than the native structure, implying that the Np state is kinetically stabilized (*56*), similar to α-lytic protease (*57*, *58*), *S. griseus* protease B (*59*), and possibly subtilisin (*60*). The present findings support the hypothesis that the native conformation is energetically disfavored, which may explain the fact that the denaturation of pepsin is an irreversible or poorly reversible (*61*) process. Further studies on the folding of pepsin and the structures of the Rp and CRp states should aid in helping to understand the underlying folding mechanisms.

ACKNOWLEDGMENT

We thank Dr. A. R. Merrill of the Department of Molecular and Cellular Biology, University of Guelph for his valuable discussions and advice on using spectrofluorophotometry and Dr. R. M. Epand, Department of Biochemistry, McMaster University for assistance with and use of the mechanical oscillating densitometer.

REFERENCES

1. Jackson, S. E. (1998) How do small single-domain proteins fold? *Folding Des. 3*, R81−R91.
2. Daggett, V., and Fersht, A., R. (2003) Is there a unifying mechanism for protein folding? *Trends Biochem. Sci.* 28, 18−25.

3. Radford, S. (2000) Protein folding: progress made and promise ahead, *Trends Biochem. Sci. 25*, 611−618.
4. Anfinsen, C. B. (1973) Principles that govern the folding of protein chains, *Science 181*, 223−230.
5. Brown, E. D., and Yada, R. Y. (1991) A kinetic and equilibrium study of the denaturation of aspartic proteinases from the fungi, *Endothia parasitica* and *Mucor miehei*, *Biochim. Biophys. Acta. 1076*, 406−415.
6. Song, J., Xu, P., Xiang, H., Su, Z., Storer, A. C., and Ni, F. (2000) The active-site residue cys-29 is responsible for the neutral-pH inactivation and the refolding barrier of human cathepsin B, *FEBS Lett. 475*, 157−162.
7. Beldarrain, A., Acosta, N., Montesinos, R., Mata, M., and Cremata, J. (2000) Characterization of *Mucor pusillus* rennin expressed in *Pichia pastoris*: enzymic, spectroscopic and calorimetric studies, *Biotechnol. Appl. Biochem. 31*, 77−84.
8. Solís-Mendiola, S., Gutiérrez-González, L. H., Arroyo-Reyna, A., Padilla-Zúñiga, J., Rojo-Domínguez, A., and Hernández-Arana, A. (1998) pH dependence of the activation parameters for chymopapain unfolding: influence of ion pairs on the kinetic stability of proteins, *Biochim. Biophys. Acta. 1388*, 363−372.
9. Baker, D., Shiau, A. K., and Agard, D. A. (1993) The role of pro regions in protein folding, *Curr. Opin. Cell Biol. 5*, 966−970.
10. Dunn, B. M. (2002) Structure and mechanism of the pepsin-like family of aspartic peptidases, *Chem. Rev. 102*, 4431−4458.
11. Richter, C., Tanaka, T., and Yada, R. Y. (1998) Mechanism of activation of the gastric aspartic proteinases: pepsinogen, progastricsin and prochymosin, *Biochem. J. 335*, 481−490.
12. Lin, X., Wong, R. N. S., and Tang, J. (1989) Synthesis, purification, and active site mutagenesis of recombinant porcine pepsinogen, *J. Biol. Chem. 264*, 4482−4489.
13. Sielecki, A. R., Fedorov, A. A., Boodhoo, A., Andreeva, N. S., and James, M. N. G. (1990) Molecular and crystal structures of monoclinic porcine pepsin refined at 1.8 A resolution, *J. Mol. Biol. 214*, 143−170.
14. Ahmad, F., and McPhie, P. (1978) Thermodynamics of the denaturation of pepsinogen by urea, *Biochemistry 17*, 241−246.
15. Frattali, V., Steiner, R. F., and Edelhoch, H. (1965) Native and unfolded states of pepsinogen. I. The molecular conformation in water and in urea, *J. Biol. Chem. 240*, 112−121.
16. Ahmad, F., and McPhie, P. (1978) The denaturation of covalently inhibited swine pepsin, *Int. J. Pept. Protein Res. 12*, 155−163.
17. McPhie, P. (1989) A reversible unfolding reaction of swine pepsin; implications for pepsinogen's folding mechanism, *Biochem. Biophys. Res. Commun. 158*, 115−119.
18. Privalov, P. L., Mateo, P. L., Khechinashvili, N. N., Stepanov, V. M., and Revina, L. P. (1981) Comparative thermodynamic study of pepsinogen and pepsin structure, *J. Mol. Biol. 152*, 445−464.
19. Lin, X. L., Loy, J. A., Sussman, F., and Tang, J. (1993) Conformational instability of the N- and C-terminal lobes of porcine pepsin in neutral and alkaline solutions, *Protein Sci. 2*, 1383−1390.
20. Tanaka, T., and Yada, R. Y. (2001) N-terminal portion acts as an initiator of the inactivation of pepsin at neutral pH, *Protein Eng. 14*, 669−674.
21. Konno, T., Kamatari, Y. O., Tanaka, N., Kamikubo, H., Dobson, C. M., and Nagayama, K. (2000) A partially unfolded structure of the alkaline-denatured state of pepsin and its implication for stability of the zymogen-derived protein, *Biochemistry 39*, 4182−4190.
22. Kamatari, Y. O., Dobson, C. M., and Konno, T. (2003) Structural dissection of alkaline-denatured pepsin, *Protein Sci. 12*, 717−724.
23. Yada, R. Y., and Nakai, S. (1986) Secondary structure of some aspartyl proteinases, *J. Food Biochem. 10*, 155−183.
24. Favilla, R., Parisoli, A., and Mazzini, A. (1997) Alkaline denaturation and partial refolding of pepsin investigated with DAPI as an extrinsic probe, *Biophys. Chem. 67*, 75−83.
25. Dunn, B. M., Jimenez, M., Parten, B. F., Valler, M. J., Rolph, C. E., and Kay, J. (1986) A systematic series of synthetic chromophoric substrates for aspartic proteinases, *Biochem. J. 237*, 899−906.
26. Svergun, D., Richard, S., Koch, M., Sayers, Z., Kuprin, S., and Zaccai, G. (1998) Protein hydration in solution: experimental observation by X-ray and neutron scattering, *Proc. Natl. Acad. Sci. U.S.A. 95*, 2267−2272.
27. Svergun, D. I. (1999) Restoring low resolution structure of biological macromolecules from solution scattering using simulated annealing, *Biophys. J. 76*, 2879−2886.
28. Svergun, D. I. (1992) Determination of the regularization parameter in indirect-transform methods using perceptual criteria, *J. Appl. Crystallogr. 25*, 495−503.
29. Svergun, D. I., Volkov, V. V., Kozin, M. B., and Stuhrmann, H. B. (1996) New developments in direct shape determination from small-angle scattering. II. Uniqueness, *Acta. Crystallogr., Sect. A 52*, 419−426.
30. Kratky, O., Leopold, H., and Stabinger, H. (1973) The determination of the partial specific volume of proteins by the mechanical oscillator technique, *Methods Enzymol. 27*, 98−110.
31. Epand, R. M., and Epand, R. F. (1980) Studies of thermotropic phospholipid phase transitions using scanning densitometry, *Chem. Phys. Lipids 27*, 139−150.
32. Liu, X. Q., and Sano, Y. (1998) Effect of Na^+ and K^+ ions on the initial crystallization process of lysozyme in the presence of D_2O and H_2O, *J. Protein Chem. 17*, 479−484.
33. Verheul, M., Roefs, S. P. F. M., and de Kruif, K. G. (1998) Aggregation of β-lactoglobulin and influence of D_2O, *FEBS Lett. 421*, 273−276.
34. Chakrabarti, G., Kim, S., Gupta, M. L., Barton, J. S., and Himes, R. H. (1999) Stabilization of tubulin by deuterium oxide, *Biochemistry 38*, 3067−3072.
35. Russo, D., Durand, D., Calmettes, P., and Desmadril, M. (2001) Characterization of the denatured states distribution of neocarzinostatin by small-angle neutron scattering and differential scanning calorimetry, *Biochemistry 40*, 3958−3966.
36. Bonnete, F., Madern, D., and Zaccai, G. (1994) Stability against denaturation mechanisms in halophilic malate dehydrogenase adapt to solvent conditions, *J. Mol. Biol. 244*, 436−447.
37. Pederson, J. S., Hansen, S., and Bauer, R. (1994) The aggregation behavior of zinc-free insulin studied by small-angle neutron scattering, *Eur. Biophys. J. 22*, 379−389.
38. Tuinier, R., and Brûlet, A. (2003) On the long-range attraction between proteins due to nonadsorbing polysaccharide, *Biomacromolecules 4*, 28−31.
39. Glatter, O. (1979) The interpretation of real-space information from small-angle scattering experiments, *J. Appl. Crystallogr. 12*, 166−175.
40. Horn, D., and Heuck, C. (1983) Charge determination of proteins with polyelectrolyte titration, *J. Biol. Chem. 258*, 1665−1670.
41. Glatter, O. (1982) Interpretation, in *Small-Angle X-ray Scattering* (Glatter, O., and Kratky, O., Eds.) pp 167−196, Academic Press: New York.
42. Glatter, O. (1977) A new method for the evaluation of small-angle scattering data, *J. Appl. Crystallogr. 10*, 415−421.
43. Kanjilal, S., Taulier, N., Le Huerou, J.-Y., Gindre, M., Urbach, W., and Waks, M. (2003) Ultrasonic studies of alcohol-induced transconformation in β-lactoglobulin: the intermediate state, *Biophys. J. 85*, 3928−3934.
44. Sreerema, N., and Woody, R. W. (1993) A self-consistent method for the analysis of protein secondary structure from circular dichroism, *Anal. Biochem. 209*, 32−44.
45. Van Stokkum, I. H. M., Spoelder, H. J. W., Bloemendal, M., Van Grondelle, R., and Groen, F. C. A. (1990) Estimation of protein secondary structure and error analysis from CD spectra, *Anal. Biochem. 191*, 110−118.
46. Manavalan, P., and Johnson, W. C., Jr. (1987) Variable selection method improves the prediction of protein secondary structure from circular dichroism spectra, *Anal. Biochem. 167*, 76−85.
47. Whitmore, L., and Wallace, B. A. (2004) DICHROWEB, an online server for protein secondary structure analyses from circular dichroism spectroscopic data, *Nucleic Acids Res. 32*, W668−W673.
48. Lobley, A., Whitmore, L., and Wallace, B. A. (2002) DICHROWEB: an interactive website for the analysis of protein secondary structure from circular dichroism spectra, *Bioinformatics 18*, 211−212.
49. Kelly, S. M., Jess, T. J., and Price, N. C. (2005) How to study proteins by circular dichroism, *Biochim. Biophys. Acta. 1751*, 119−139.
50. Lakowicz, J. R. (2000) *Topics in Fluorescence Spectroscopy: Protein Fluorescence.* Kluwer Academic/Plenum Publishers, New York.
51. Burstein, E. A., Vedenkina, N. S., and Ivkova, M. N. (1973) Fluorescence and the location of tryptophan residues in protein molecules, *Photochem. Photobiol. 18*, 263−279.
52. Privalov, P. L., and Potekhin, S. A. (1986) Scanning microcalorimetry in studying temperature-induced changes in proteins, *Methods Enzymol. 131*, 4−51.

53. Yoshimasu, M. A., Tanaka, T., Ahn, J.- K., and Yada, R. Y. (2004) Effect of N-linked glycosylation on the aspartic proteinase porcine pepsin expressed from *Pichia pastoris*, *Glycobiology 14*, 417−429.
54. O'Brian, R., and Haq, I. (2004) Applications of Biocalorimetry: Binding, Stability and Enzyme Kinetics, in *Biocalorimetry II: Applications of Calorimetry in the Biological Sciences* (Ladbury, J. E., and Doyle, M. L., Eds.) pp 1−34, John Wiley & Sons, Ltd., West Sussex, England.
55. Baker, D., and Agard, D. A. (1994) Kinetics versus thermodynamics in protein folding, *Biochemistry 33*, 7505−7509.
56. Jaswal, S. S., Truhlar, S. M., Dill, K. A., and Agard, D. A. (2005) Comprehensive analysis of protein folding activation thermodynamics reveals a universal behavior violated by kinetically stable proteases, *J. Mol. Biol. 347*, 355−366.
57. Sohl, J. L., Jaswal, S. S., and Agard, D. A. (1998) Unfolded conformations of alpha-lytic protease are more stable than its native state, *Nature 395*, 817−819.
58. Baker, D., Sohl, J. L., and Agard, D. A. (1992) A protein-folding reaction under kinetic control, *Nature 356*, 263−265.
59. Truhlar, S. M. E., Cunningham, E. L., and Agard, D. A. (2004) The folding landscape of *Streptomyces griseus* protease B reveals the energetic costs and benefits associated with evolving kinetic stability, *Protein Sci. 13*, 381−390.
60. Eder, J., Rheinnecker, M., and Fersht, A. R. (1993) Folding of subtilisin BPN′: characterization of a folding intermediate, *Biochemistry 32*, 18−26.
61. Kurimoto, E., Harada, T., Akiyama, A., Sakai, T., and Kato, K. (2001) In vitro refolding of porcine pepsin immobilized on agarose beads, *J. Biochem. 130*, 295−297.

BI061270I